THE JOURNAL OF PHYSICAL CHEMISTRY C

Article

pubs.acs.org/JPCC

STM and STS Studies on the Density of States Modulation of $Pr@C_{82}$ and $Sc_3C_2@C_{80}$ Binary-Metallofullerene Peapods

Yuki Iijima,[†] Kazunori Ohashi,[†] Naoki Imazu,[†] Ryo Kitaura,[†] Ken Kanazawa,[‡] Atsushi Taninaka,[‡] Osamu Takeuchi,[‡] Hidemi Shigekawa,[‡] and Hisanori Shinohara*,[†]

[†]Department of Chemistry and Institute for Advanced Research, Nagoya University, Nagoya, Aichi 464-8602, Japan

[‡]Graduate School of Pure and Applied Sciences, University of Tsukuba, 1-1-1 Tennodai, Tsukuba 305-8571, Japan

Supporting Information

ABSTRACT: The density of states modulation of single-wall carbon nanotubes (SWCNTs) is induced by the encapsulation of two different kinds of metallofullerenes ($Pr@C_{82}$ and $Sc_3C_2@C_{80}$). We report the observation of the modulated density of states using scanning tunneling microscopy/spectroscopy, where the modulation is successfully reproduced by density functional theory calculation. The metallofullerene molecules in SWCNTs strongly affect the local band structures of SWCNTs. The present findings show that the local electronic structures of SWCNTs can be modified by not only varying the geometric structures of SWCNTs but also the varieties of metallofullerenes encapsulated.

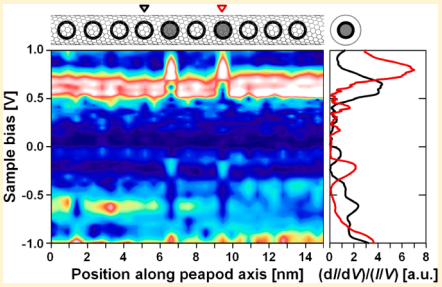

INTRODUCTION

Single-wall carbon nanotubes (SWCNTs) have been attracting considerable interest due to their promising potential to miniaturize electronics beyond the current scale of micro-electromechanical systems as a result of their inherent nanoscale structures and unique electronic properties.[1,2] In particular, their band gap can be varied between 0 and 1.5 eV by varying their geometrical structure, while their electrical conductivity can exhibit metallic or semiconducting behavior depending on their chirality. To apply SWCNTs to nano-electronic devices such as field-effect transistors[3] and sensors,[4] it is critical to control their electronic structures.

One of the most effective ways to realize this is to encapsulate atoms or molecules such as fullerenes and endohedral metallofullerenes[5] in their central hollow spaces.[6−9] Electron microscopy studies have revealed the one-dimensional alignment of metallofullerenes inside CNTs.[6,10] Encapsulation of C_{60} induces a diameter-dependent variation in the band gap of SWCNTs[11] so that their photoluminescence properties vary with their diameters.[12] We found that the encapsulating $Gd@C_{82}$ metallofullerenes had significantly reduced the band gap of SWCNTs.[7] In addition, the field-effect transistor characteristics of SWCNTs encapsulating $Gd@C_{82}$ molecules (known as metallofullerene peapods) exhibit ambipolar characteristic that differ completely from those of the conventional empty SWCNTs.[8] We also found that the band gap modulation of SWCNTs in fullerene peapods strongly depends on the fullerenes used.[13] These studies clearly demonstrate that the peapod formation is an effective way to control the electronic band structure of SWCNTs. However, to date the details of the mechanism for the change in the electronic structure have not sufficiently been understood.

We have so far reported that the two main factors determining the electronic structure of peapods are the encapsulated metallofullerene and the chirality of carbon nanotubes (CNTs). In this respect, atomic resolution scanning tunneling microscopy/spectroscopy (STM/STS) observation of the electronic local density of states (DOS) near the Fermi level is a powerful method to investigate the electronic structures of CNTs[14,15] and peapods.[7,11] The defects on the CNT surface show localized states in the band gap of the CNT.[14,16] We found moiré patterns showing local electronic modulations of double-wall CNTs.[15] Substantial spatial band gap modification of SWCNTs was observed in a low-temperature STM/STS investigation of $Gd@C_{82}$ peapods. We found that the band gap of 0.5 eV was reduced to 0.1 eV when $Gd@C_{82}$ fullerenes were tightly encapsulated in small-diameter SWCNTs.[7] This band gap reduction occurs locally at the locations of $Gd@C_{82}$ metallofullerenes encapsulated. In the previous study, we observe a band gap reduction only for a $Gd@C_{82}$@(11, 9) SWCNT peapod. To further shed light on the origin of the band gap modulation of SWCNTs encapsulating various fullerenes or metallofullerenes, it is necessary to study the electronic local band structures of metallofullerene peapods having similar chiralities.

In the present study, we encapsulate two different kinds of metallofullerenes in the same SWCNT, the binary-metallofullerene peapods. The two different metallofullerenes encapsulated might induce two different modifications in the electronic structure of the SWCNT. STM/STS analyses of such binary-metallofullerene peapods thus enable us to investigate

Received: December 29, 2012
Revised: March 14, 2013
Published: March 20, 2013

dx.doi.org/10.1021/jp3128466 | J. Phys. Chem. C 2013, 117, 6966−6971

metallofullerene-dependent DOS modulation of SWCNTs in a single peapod without considering the chirality dependence. Here, we report a STM/STS study on binary-metallofullerene peapods, in which Pr@C_{82} and Sc_3C_2@C_{80} are encapsulated in the exactly same SWCNT. STM/STS measurements are performed by low-temperature STM (LT-STM) under ultra-high vacuum (UHV) at 5 K. In addition, we performed density functional theory (DFT) band structure calculations to analyze the observed STM/STS results.

EXPERIMENTAL SECTION

Experimental Procedures. SWCNTs were synthesized by the enhanced direct-injection pyrolytic synthesis (e-DIPS) method.[17] The SWCNT sample was purified by thermal oxidation at 773 K for 30 min in an electric furnace followed by high-temperature vacuum heat treatment at 1473 K for 12 h in an infrared furnace. The average diameter of the SWCNT is estimated to be 1.6 nm with a standard deviation of 0.2 nm from high-resolution transmission electron microscopy (HRTEM) observations. Prior to the encapsulation of metallofullerenes in SWCNTs, the SWCNTs were heated in dry air at 823 K for 30 min in an electric furnace to open the tube ends.

Pr@C_{82} and Sc_3C_2@C_{80} metallofullerenes were synthesized by DC arc discharge and were purified by multistage high-performance liquid chromatography (HPLC)[5] using toluene as the eluent. The purities of Pr@C_{82} and Sc_3C_2@C_{80} metallofullerenes were checked by positive and negative laser desorption time-of-flight mass spectrometry and by HPLC analyses.

The Pr@C_{82} and Sc_3C_2@C_{80} metallofullerenes were encapsulated in SWCNTs by a gas-phase reaction.[18] Isolated Pr@C_{82} and Sc_3C_2@C_{80} metallofullerenes and the open-ended SWCNTs were placed in a quartz tube and vacuum sealed to 2.0×10^{-7} Torr at 573 K for 1 h. The quartz tube was then heated at 823 K for 3 days in the electric furnace to encapsulate Pr@C_{82} and Sc_3C_2@C_{80} metallofullerenes in SWCNTs.

Au(111) substrates were purchased from Unisoku Co., Ltd.. The Au(111) substrates were flame annealed in air prior to deposition. The binary-metallofullerene peapods were dispersed in 1,2-dichloroethane by sonication for more than 10 h. After sonication, 10 drops of the dispersion solution were deposited by drop casting to the Au(111) substrates at 573 K. The samples were annealed at 573 K for 1 h before introducing into an UHV-STM chamber.

The STM/STS measurements were performed at 5 K under UHV conditions (base pressure $<7.5 \times 10^{-11}$ Torr) using an Omicron UHV LT-STM system in constant-current mode operated using an electrochemically sharpened tungsten tip. This STM system has a thermal drift of less than 0.002 nm/s. We used the WSxM software to process the obtained STM images.[19]

Calculation Details. Theoretical calculations were performed on the structures and electronic properties of the SWCNTs, Pr@C_{82} peapods, and Sc_3C_2@C_{80} peapods. All calculations were performed based on DFT using the Vienna ab initio simulation package (VASP).[20,21] In these calculations, we used the generalized gradient approximation (GGA) and a plane-wave basis set with a cutoff energy of 250 eV since this cutoff energy has been reported to provide reliable results for the present purpose.[22] The interaction between the ionic cores and the valence electrons was implemented through the projector augmented wave (PAW) method.[23] We treat all four ($2s^2 2p^2$), three ($3d^2 4s$), and 11 ($5s^2 5p^6 5d6s^2$) valence electrons of carbon (C), scandium (Sc), and praseodymium (Pr), respectively. The atomic positions are relaxed with residual Hellman–Feynman forces smaller than 0.01 eV/Å by using the conjugate gradient method incorporating one irreducible k-point with the coordinate $(0, 0, 1/4)(2\pi/T)$, where T is the translational period.

Band structure calculations were fully performed self-consistently using 101 irreducible k-points for SWCNTs $[(0, 0, n/200)(2\pi/T)$, $n = 0, 1,..., 100]$ and 21 irreducible k-points for metallofullerene peapods (Pr@C_{82} and Sc_3C_2@C_{80} peapods) $[(0, 0, n/40)(2\pi/T)$, $n = 0, 1,..., 20]$. Gaussian smearing with a parameter of $\sigma = 0.02$ eV was applied to broaden the one-electron eigenenergies. The metallofullerenes were found to be repeatedly placed along the CNT axis with an intermolecular distance of approximately 1 nm, which is equal to the periodicity of the SWCNT. For STS calculations, we used partial (band decomposed) charge densities that correspond to the local DOS.

RESULTS AND DISCUSSION

HRTEM and EDX Characterization of Binary Metallofullerene Peapods. Figure 1a shows a HRTEM image of a bundle of (Pr@C_{82} and Sc_3C_2@C_{80})$_n$@SWCNTs peapods. It clearly shows that the metallofullerenes are densely packed in the SWCNTs, giving rise to the formation of a one-dimensional crystalline array. The metallofullerenes are estimated to have a filling ratio of typically over 90% from the observed HRTEM images.

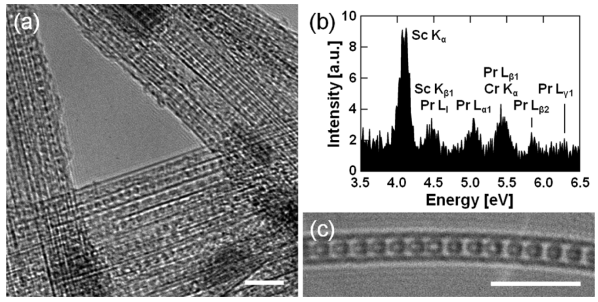

Figure 1. HRTEM images and EDX spectra of binary-metallofullerene peapods: (Pr@C_{82} and Sc_3C_2@C_{80})$_n$@SWCNTs. (a) HRTEM image of binary-metallofullerene peapod bundles, (b) EDX spectra of binary-metallofullerene peapods in panel a, and (c) HRTEM image of isolated binary-metallofullerene peapod. The scale bars in both TEM images are 5 nm.

Figure 1b shows an energy-dispersive X-ray (EDX) spectrum measured in the exactly same area shown in Figure 1a. The $L_{\alpha1}$ (5.03 keV), $L_{\beta2}$ (5.85 keV), and $L_{\gamma1}$ (6.32 keV) emission lines of Pr are all spectrally resolved. The $L_{\beta1}$ (5.49 keV) emission line of Pr is obscured by the K_α (5.42 keV) line of chromium (Cr), which is attributed to the contamination from the ultrasonication tip used for dispersion when preparing the TEM sample. The L_l (4.45 keV) line of Pr is also indicated but it overlaps with $K_{\beta1}$ Sc emission. For Sc, lines corresponding to K_α (α_1 and α_2 at 4.09 keV) and $K_{\beta1}$ (4.46 keV) emissions are present as indicated in the spectrum but only the K_α doublet is spectrally resolved. A strong correlation is found between the positions of the Pr and Sc lines of (Pr@C_{82} and Sc_3C_2@C_{80})$_n$@SWCNT in Figure 1b and those of PrSc@C_{80}.[24] Therefore, we can identify the peapods in Figure 1a to be the binary-

dx.doi.org/10.1021/jp3128466 | J. Phys. Chem. C 2013, 117, 6966–6971

metallofullerene peapods (Pr@C_{82} and Sc_3C_2@C_{80})$_n$@SWCNTs. Moreover, the ratio of Pr@C_{82} to Sc_3C_2@C_{80} metallofullerenes in SWCNTs is estimated to be 1.0:5.2 based on the intensities of Sc K_α, Pr $L_{\alpha1}$, Pr $L_{\beta2}$, and Pr $L_{\gamma1}$ emissions in Figure 1b.

Figure 1c shows an HRTEM image of an isolated binary-metallofullerene peapod. The intermolecular distance is about 1.1 nm, which is reasonable for the van der Waals separation generally observed in C_{80} and C_{82} fullerenes,[6,25] indicating that this intermolecular distance corresponds to the monomeric form of C_{80} or C_{82}.

STM Image and Position-Dependent STS Mapping of Peapods. Figure 2a shows a schematic diagram of an individual binary-metallofullerene peapod. The abscissas in Figures 2a–c indicate the position along the peapod axis, where the two kinds of metallofullerene molecules are aligned with each other. The open and filled circles in Figure 2a denote the Pr@C_{82} and Sc_3C_2@C_{80} metallofullerenes, respectively, as inferred from an intensity plot obtained from the STS spectra taken along the peapod axis (Figure 2c). STM/STS (dI/dV, where I is the current and V is the voltage) provides bias-dependent topographic images and the local DOS. Figure 2b shows a typical STM topographic image of a binary-metallofullerene peapod, (Pr@C_{82} and Sc_3C_2@C_{80})$_n$@SWCNT, obtained with a bias voltage of +1.0 V and a set point current of +1.0 nA. This STM topographic image was obtained by using 512 × 512 pixels to image a 25 × 25 nm^2 region; thus, the STM topographic imaging has a resolution of 0.049 nm in the horizontal (x) and vertical (y) directions. As Figure 2b clearly shows, a typical lattice image originating from the atomic lattice of SWCNT was observed. The chiral angle[26,27] (i.e., the angle between the hexagon rows and the CNT axis) is estimated to be 11–14° from the atomically resolved STM image. The SWCNT diameter is estimated to be 1.4–1.6 nm based on the apparent height and width of the SWCNT. On the basis of these estimates for the chiral angle and diameter, the chiral indices of the SWCNT are estimated to be (15, 5), (16, 5), and (17, 5).

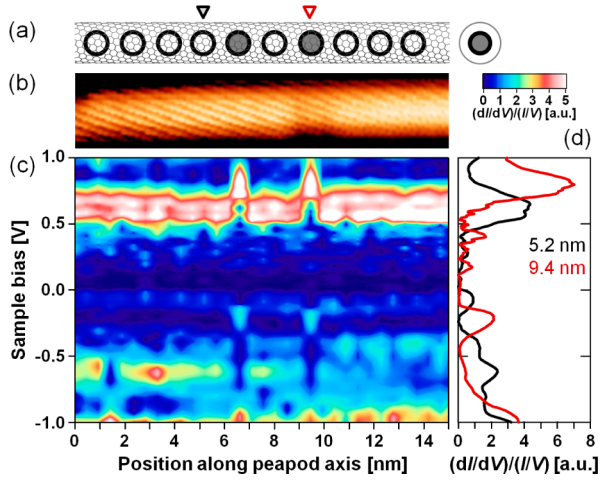

Figure 2. (a) Schematic diagram of a binary-metallofullerene peapod. (b) STM topographic image (V_s = +1.0 V; I_t = +1.0 nA). (c) Intensity plot obtained from the STS spectra as a function of voltage bias (ordinate) and position along the peapod (abscissa). (d) Two representative $(dI/dV)/(I/V)$ spectra (black and red lines) as a function of bias obtained from the two locations indicated by the triangles in (a). The color scale indicates the normalized differential conductance $(dI/dV)/(I/V)$.

In the STM topographic images of the binary-metallofullerene peapods obtained at the bias voltages of +1.0, +1.2, and −1.2 V, no modulations due to modification of the local electronic structure by the encapsulated metallofullerenes were observed besides that for the atomic lattice of SWCNT. Therefore, the exact locations of the encapsulated metallofullerenes cannot be determined solely from these STM images. To observe the local variation of the electronic structure, we performed site-dependent STS measurements on the binary-metallofullerene peapods. Since minimizing the thermal drift during measurements is crucial to obtain reliable results, STM/STS measurements were performed with a thermal drift of less than 0.002 nm/s. Figure 2c shows an intensity plot obtained from the STS spectra taken along the peapod axis. The STM topographic imaging was performed by using 512 × 512 pixels to image a 30 × 30 nm^2 region, whereas the STS spectra were obtained at every four pixels with eight lines along the x and y direction, respectively. The STS spectral resolutions in the x and y directions are 0.234 and 0.469 nm, respectively. There are 400 data points between −1.522 and +1.522 V; the bias interval is thus 0.0076 V. The ordinate in Figure 2c indicates the sample voltage bias. The normalized differential conductance $(dI/dV)/(I/V)$ shown in Figure 2c corresponds to the local DOS at each position.[28]

As is clearly seen in Figure 2c, two DOS features located at 6.6 and 9.4 nm along the peapod axis differ distinctly from those at other positions. When we performed the STS measurements at a large defect-like hole on the CNT surface, we normally observed this kind of DOS shift. However, since this STM topographic image does not show any evidence of defects, we infer that these DOS shifts exhibiting similar shapes do not originate from CNT surface defects. Moreover, these shifted DOS are separated by 2.8 nm, which is twice as large as the intermolecular distance (see Supporting Information). These results thus suggest the presence of an array of the Pr@C_{82} and Sc_3C_2@C_{80} metallofullerenes with an interval of 1.4 nm and the intensity difference is due to the local DOS modulation resulting from the two different metallofullerenes. However, this DOS shift could not be directly observed in the current study.

Figure 2d shows the representative $(dI/dV)/(I/V)$ spectra (black and red lines) as a function of bias voltage obtained from two locations (5.2 and 9.4 nm, as indicated by the two triangles in Figure 2a) along the peapod axis. From Figures 2c and d) and Table 1, the positions of the first van Hove singularity (vHs) peak in the conduction band (peak 2) and the valence

Table 1. vHs Peak Positions and Shifts[a]

	fullerene 1 (V)	fullerene 2 (V)
peak 1 in C	+0.79	+0.61
Δ1	+0.18	
peak 2 (1st–vHs) in C	+0.17	+0.28
Δ2	−0.11	
peak 3 (1st–vHs) in V	−0.20	−0.07
Δ3	−0.13	

[a]Peaks 1 and 2 in C and peak 3 in V indicate the positions of the vHs peak at 9.4 nm (fullerene 1) and 5.2 nm (fullerene 2) along the peapod axis. Δ1 and Δ2 indicate the difference in the positions of the vHs peak (fullerene 1 − fullerene 2).

dx.doi.org/10.1021/jp3128466 | J. Phys. Chem. C 2013, 117, 6966–6971

band (peak 3) at 9.4 nm, which is estimated to be above one of the two metallofullerenes (fullerene 1, denoted by filled circles), are shifted by −0.11 V (from +0.28 to +0.17 V) and by −0.13 V (from −0.07 to −0.20 V) relative to that at 5.2 nm, which is estimated to be above the other metallofullerene (fullerene 2, denoted by open circles), respectively. The position of the vHs peak in the conduction band (peak 1) at 9.4 nm above fullerene 1, shifts by +0.18 V from 0.61 to 0.79 V relative to that at 5.2 nm above fullerene 2. We infer that the peak energy positions depend on the metallofullerene. In addition to these shifts in the vHs peak positions, DOS gaps are observed. The DOS intensity between −0.34 and −0.74 V in the valence band at 6.6 and 9.4 nm is weaker than that at other positions along the peapod axis. These DOS modulations are, therefore, considered to originate from the two different metallofullerenes.

First-Principles Calculations (STS Two-Dimensional Plot). To investigate the origin of the DOS energy shift shown in Figure 2, we performed DFT calculations on the STS intensities of SWCNT, Pr@C_{82} peapod, and Sc_3C_2@C_{80} peapod. As discussed above, there are three possible chiralities for the SWCNTs in (Pr@C_{82} and Sc_3C_2@C_{80})$_n$@SWCNT: (15, 5), (16, 5), and (17, 5). In the present DFT calculations, we chose (15, 5) SWCNT due to the computational limitation that the translational vector along the CNT axis should have a similar size to that of metallofullerenes under periodic boundary conditions. A (15, 5) SWCNT of 1.43 nm in diameter has the chiral angle of 13.9° and a translation vector length of 1.56 nm. Figures 3a−c shows the calculated STS intensity plots and the corresponding structure models of (15, 5) SWCNT, Pr@C_{82}@(15, 5) peapod, and Sc_3C_2@C_{80}@(15, 5) peapod, respectively. The initial atomic positions in the metallofullerenes used for structural optimization are those obtained from an X-ray diffraction study of M@C_{82} and Sc_3C_2@C_{80}.[29] The C_2 axis of the C_{82}−C_{2v} cage and the S_{10} axis of the C_{80}−I_h cage are placed perpendicular and parallel to the CNT axis, respectively. The top and middle rows in Figure 3 show the atomic positions of the structural models after structural optimization.

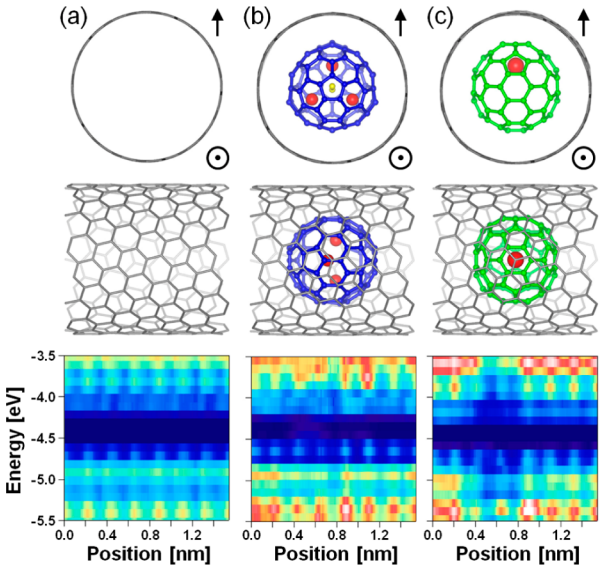

Figure 3. Calculated STS intensity plots for (a) (15, 5) SWCNT, (b) Sc_3C_2@C_{80}@(15, 5), and (c) Pr@C_{82}@(15, 5) peapods. The top and middle rows show the structural models. (15, 5) SWCNTs are shown in gray. Fullerene C_{80}, Sc atoms, and C atoms are shown in blue, red, and yellow, respectively. Fullerene C_{82} and Pr atoms are shown in green and red, respectively. The bottom row shows two-dimensional map of calculated dI/dV spectra as a function of energy (ordinate) and the position of the STM tip along the CNT (abscissa). The arrows in the top row indicate the theoretical STM tip direction.

As mentioned in the Experimental Section, we used the partial charge densities calculated by VASP for the STS calculations. We have to emphasize here that the STS measures the tail of the wave function rather than the usual DOS at the atomic position.[30] The charge density corresponds to the norm of the wave function. The partial charge densities are calculated at a distance of 3.3 Å above the CNT surface along the CNT length. To simulate the actual resolution of the STM tip, they are averaged across a 7.3 Å long horizontal line perpendicular to the CNT axis.

The bottom row in Figure 3 shows the calculated STS intensity plots, which provide more extensive data as a function of energy (ordinate) and position of the tip along the CNT axis (abscissa). In addition, we set the vacuum level to zero to compare the vHs peak positions of SWCNT and peapod DOS. These normalized STS intensity plots indicate the calculated local DOS near the Fermi level of the CNT surface modified by the encapsulating metallofullerenes. These local DOS modulations strongly depend on the metallofullerene used. Regardless of the tip position (i.e., irrespective of whether the tip was above or between the metallofullerenes), we observed negative shifts in the first-vHs peak positions of Pr@C_{82}@(15, 5) peapod in both the conduction and valence bands as compared with those of (15, 5) SWCNT and Sc_3C_2@C_{80}@(15, 5) peapod in Figures 3a and b, respectively. In addition to these calculated DOS shifts, DOS gaps are also observed. The DOS intensities in both the conduction and valence bands above the Pr atom in the Pr@C_{82}@(15, 5) peapod are weaker than those of the (15, 5) SWCNT and the Sc_3C_2@C_{80}@(15, 5) peapod.

These results exhibit good agreement with the experimental results shown in Figures 2c and d. We therefore conclude that the experimental results can be attributed to the local DOS modulation of SWCNTs by the encapsulating two different metallofullerenes. On the basis of the results above, one of the two metallofullerenes at the two DOS features observed at 6.6 and 9.4 nm along the peapod axis differ distinctly from those at other positions in Figure 2c and are thus considered to be Pr@C_{82} metallofullerenes.

First-Principles Calculations (One-Dimensional DOS Plot). Figure 4 shows the site-projected DOS of (15, 5) SWCNT, Sc_3C_2@C_{80}@(15, 5) and Pr@C_{82}@(15, 5) peapods. Comparison of Figure 4c with Figures 4a and b reveals that the DOS configuration of (15, 5) in Pr@C_{82}@(15, 5) peapod is integrally shifted by about 0.09 eV in the negative direction. For example, the first vHs peak positions in the conduction band (peak 2) and valence band (peak 3) of (15, 5) in Pr@C_{82}@(15, 5) peapod shift by 0.08 V (from −4.17 to 4.25 V) and 0.11 V (from −4.63 to −4.74 V) relative to that of (15, 5) in Sc_3C_2@C_{80}@(15, 5) peapod, respectively (see Table 2). The difference in the relative peak positions of the (15, 5) SWCNT in the Pr@C_{82}@(15, 5) peapod and the (15, 5) SWCNT in the Sc_3C_2@C_{80}@(15, 5) peapod relative to the vacuum level has important implications for the experimental results shown in Figures 2c and d. Namely, these negative shifts can be interpreted as the relative reduction in the energies of the electrons in the (15, 5) SWCNT due to the effect of the local electrostatic potential from the Pr@C_{82} metallofullerene originating from the

dx.doi.org/10.1021/jp3128466 | J. Phys. Chem. C 2013, 117, 6966−6971

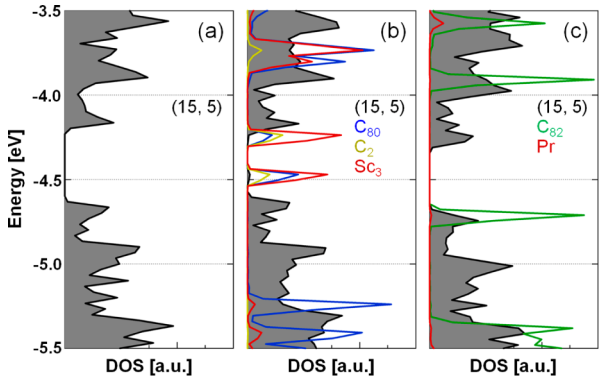

Figure 4. Site-projected density of states (pDOS) of (a) (15, 5) SWCNT, (b) $Sc_3C_2@C_{80}@(15, 5)$, and (c) $Pr@C_{82}@(15, 5)$ peapods decomposed in their constituents. Gray regions contained in black lines denote the pDOS of (15, 5) SWCNT. Blue, yellow, and red lines in (b) denote the pDOS of fullerene C_{80}, C atoms, and Sc atoms, respectively. Green and red lines in (c) denote the pDOS of fullerene C_{82} and Pr atom, respectively.

Table 2. Positions and shift of vHs peaks[a]

	empty (eV)	$Sc_3C_2@C_{80}$ (eV)	$Pr@C_{82}$ (eV)
peak 1 (2nd−vHs) in C	−3.89	−3.89	−3.97
Δ1	0		−0.08
peak 2 (1st−vHs) in C	−4.17	−4.17	−4.25
Δ2	0		−0.08
peak 3 (1st−vHs) in V	−4.66	−4.63	−4.74
Δ3	−0.03		−0.11
peak 4 (2nd−vHs) in V	−4.91	−4.91	−5.01
Δ4	0		−0.10

[a]Peaks 1−4 indicate the positions of the second and the first vHs peaks in conductance band and first and second vHs peaks in valence band, respectively. Δ1−Δ4 indicate the differences in the positions of the vHs peaks of (15, 5) SWCNT and $Pr@C_{82}@(15, 5)$ peapod − $Sc_3C_2@C_{80}@(15, 5)$ peapod.

difference in the electrical charge distributions of $Pr@C_{82}$ and $Sc_3C_2@C_{80}$ metallofullerenes. As a result, the position of the DOS is shifted, whereas the shape of the DOS does not change.

The lowest unoccupied molecular orbital (LUMO) of $Sc_3C_2@C_{80}$ is located in the middle of the CNT gap according to Figure 4b. In this small bias range, we assume that this LUMO state evades the STS tip in the present experiments, partly because it has a low tunneling probability. The C_{80} state at −4.47 eV is hardly visible because this state has a short decay length in the theoretical STM tip direction.

CONCLUSION

We used LT-STM/STS to observe the electronic states modification of SWCNTs, which is induced by encapsulating two different kinds of metallofullerenes. To observe the metallofullerene-dependent DOS modulation of SWCNTs without considering the chirality dependence, we used binary-metallofullerene peapods that encapsulate two different metallofullerenes, the $Pr@C_{82}$ and $Sc_3C_2@C_{80}$ molecules, in an identical SWCNT. From the experimental results and DFT calculations, we successfully determined the positions of $Pr@C_{82}$ and $Sc_3C_2@C_{80}$ in the SWCNTs. The STS results reveal that the DOS shifts originate from the encapsulation of the two different metallofullerenes. We found that the relative positions of the conduction band and valence band peaks vary depending on the metallofullerene encapsulated. This variation is thought to be due to the local electrostatic potential from different electrical charge distributions of $Pr@C_{82}$ and $Sc_3C_2@C_{80}$ in SWCNTs.

ASSOCIATED CONTENT

Supporting Information

Intensity plot obtained from the STS spectra taken along peapod axis. Atomic positions of metallofullerenes prior to optimization. This material is available free of charge via the Internet at http://pubs.acs.org.

AUTHOR INFORMATION

Corresponding Author

*Tel.: +81 52 789 2482. Fax: +81 52 747 6442. E-mail: noris@nagoya-u.jp.

Notes

The authors declare no competing financial interest.

ACKNOWLEDGMENTS

This work has been supported by Grant-in-Aids for Specific Area Research (No. 19084008) on Carbon Nanotube Nanoelectronics and for Scientific Research A (No. 19205003) from MEXT, Japan, and the Global COE Program in Chemistry, Nagoya University.

REFERENCES

(1) Iijima, S. *Nature* **1991**, *354*, 56−58.
(2) Saito, R.; Fujita, M.; Dresselhaus, G.; Dresselhaus, M. S. *Appl. Phys. Lett.* **1992**, *60*, 2204−2206.
(3) Tans, S. J.; Verschueren, A. R. M.; Dekker, C. *Nature* **1998**, *393*, 49−52.
(4) Kong, J.; Franklin, N. R.; Zhou, C.; Chapline, M. G.; Peng, S.; Cho, K.; Dai, H. *Science* **2000**, *287*, 622−625.
(5) Shinohara, H. *Rep. Prog. Phys.* **2000**, *63*, 843−892.
(6) Hirahara, K.; Suenaga, K.; Bandow, S.; Kato, H.; Okazaki, T.; Shinohara, H.; Iijima, S. *Phys. Rev. Lett.* **2000**, *85*, 5384−5387.
(7) Lee, J.; Kim, H.; Kahng, S. J.; Kim, G.; Son, Y. W.; Ihm, J.; Kato, H.; Wang, Z. W.; Okazaki, T.; Shinohara, H.; Kuk, Y. *Nature* **2002**, *415*, 1005−1008.
(8) Shimada, T.; Okazaki, T.; Taniguchi, R.; Sugai, T.; Shinohara, H.; Suenaga, K.; Ohno, Y.; Mizuno, S.; Kishimoto, S.; Mizutani, T. *Appl. Phys. Lett.* **2002**, *81*, 4067−4069.
(9) Ohashi, K.; Imazu, N.; Kitaura, R.; Shinohara, H. *J. Phys. Chem. C* **2011**, *115*, 3968−3972.
(10) Suenaga, K.; Sato, Y.; Liu, Z.; Kataura, H.; Okazaki, T.; Kimoto, K.; Sawada, H.; Sasaki, T.; Omoto, K.; Tomita, T.; Kaneyama, T.; Kondo, Y. *Nature Chem.* **2009**, *1*, 415−418.
(11) Hornbaker, D. J.; Kahng, S. J.; Misra, S.; Smith, B. W.; Johnson, A. T.; Mele, E. J.; Luzzi, D. E.; Yazdani, A. *Science* **2002**, *295*, 828−831.
(12) Okubo, S.; Okazaki, T.; Kishi, N.; Joung, S.-K.; Nakanishi, T.; Okada, S.; Iijima, S. *J. Phys. Chem. C* **2008**, *113*, 571−575.
(13) Shimada, T.; Ohno, Y.; Suenaga, K.; Okazaki, T.; Kishimoto, S.; Mizutani, T.; Taniguchi, R.; Kato, H.; Cao, B.; Sugai, T.; Shinohara, H. *Jpn. J. Appl. Phys.* **2005**, *44*, 469−472.
(14) Berthe, M.; Yoshida, S.; Ebine, Y.; Kanazawa, K.; Okada, A.; Taninaka, A.; Takeuchi, O.; Fukui, N.; Shinohara, H.; Suzuki, S.; Sumitomo, K.; Kobayashi, Y.; Grandidier, B.; Stiévenard, D.; Shigekawa, H. *Nano Lett.* **2007**, *7*, 3623−3627.
(15) Fukui, N.; Suwa, Y.; Yoshida, H.; Sugai, T.; Heike, S.; Fujimori, M.; Terada, Y.; Hashizume, T.; Shinohara, H. *Phys. Rev. B* **2009**, *79*, 125402.
(16) Lee, S.; Kim, G.; Kim, H.; Choi, B.-Y.; Lee, J.; Jeong, B. W.; Ihm, J.; Kuk, Y.; Kahng, S.-J. *Phys. Rev. Lett.* **2005**, *95*, 166402.
(17) Saito, T.; Ohshima, S.; Okazaki, T.; Ohmori, S.; Yumura, M.; Iijima, S. *J. Nanosci. Nanotechnol.* **2008**, *8*, 6153−6157.

(18) Kitaura, R.; Shinohara, H. *Chem.—Asian J.* **2006**, *1*, 646−655.
(19) Horcas, I.; Fernandez, R.; Gomez-Rodriguez, J. M.; Colchero, J.; Gomez-Herrero, J.; Baro, A. M. *Rev. Sci. Instrum.* **2007**, *78*, 013705.
(20) Kresse, G.; Furthmueller, J. *Comput. Mater. Sci.* **1996**, *6*, 15−50.
(21) Kresse, G.; Furthmueller, J. *Phys. Rev. B* **1996**, *54*, 11169−11186.
(22) Dubay, O.; Kresse, G. *Phys. Rev. B* **2004**, *70*, 165424.
(23) Kresse, G.; Joubert, D. *Phys. Rev. B* **1999**, *59*, 1758−1775.
(24) Plant, S. R.; Ng, T. C.; Warner, J. H.; Dantelle, G.; Ardavan, A.; Briggs, G. A. D.; Porfyrakis, K. *Chem. Commun.* **2009**, 4082−4084.
(25) Smith, B. W.; Luzzi, D. E.; Achiba, Y. *Chem. Phys. Lett.* **2000**, *331*, 137−142.
(26) Wilder, J. W. G.; Venema, L. C.; Rinzler, A. G.; Smalley, R. E.; Dekker, C. *Nature* **1998**, *391*, 59−62.
(27) Odom, T. W.; Huang, J.-L.; Kim, P.; Lieber, C. M. *Nature* **1998**, *391*, 62−64.
(28) Feenstra, R. M.; Stroscio, J. A.; Fein, A. P. *Surf. Sci.* **1987**, *181*, 295−306.
(29) Nishibori, E.; Terauchi, I.; Sakata, M.; Takata, M.; Ito, Y.; Sugai, T.; Shinohara, H. *J. Phys. Chem. B* **2006**, *110*, 19215−19219.
(30) Cho, Y.; Han, S.; Kim, G.; Lee, H.; Ihm, J. *Phys. Rev. Lett.* **2003**, *90*, 106402.